Dynamic and thermodynamic properties of the generalised diamond chain model for azurite

Andreas Honecker[1], Shijie Hu[1], Robert Peters[2] and Johannes Richter[3]

[1] Institut für Theoretische Physik, Georg-August-Universität Göttingen, 37077 Göttingen, Germany

[2] Department of Physics, Graduate School of Science, Kyoto University, Kyoto 606-8502, Japan

[3] Institut für Theoretische Physik, Otto-von-Guericke-Universität Magdeburg, P.O. Box 4120, 39016 Magdeburg, Germany

E-mail: ahoneck@uni-goettingen.de

Abstract. The natural mineral azurite $Cu_3(CO_3)_2(OH)_2$ is an interesting spin-1/2 quantum antiferromagnet. Recently, a generalised diamond chain model has been established as a good description of the magnetic properties of azurite with parameters placing it in a highly frustrated parameter regime. Here we explore further properties of this model for azurite. First, we determine the inelastic neutron scattering spectrum in the absence of a magnetic field and find good agreement with experiments, thus lending further support to the model. Furthermore, we present numerical data for the magnetocaloric effect and predict that strong cooling should be observed during adiabatic (de)magnetisation of azurite in magnetic fields slightly above 30T. Finally, the presence of a dominant dimer interaction in azurite suggests the use of effective Hamiltonians for an effective low-energy description and we propose that such an approach may be useful to fully account for the three-dimensional coupling geometry.

PACS numbers: 75.10.Jm, 75.30.Sg, 02.70.-c, 78.70.Nx

Published as: *J. Phys.: Condens. Matter* **23** (2011) 164211

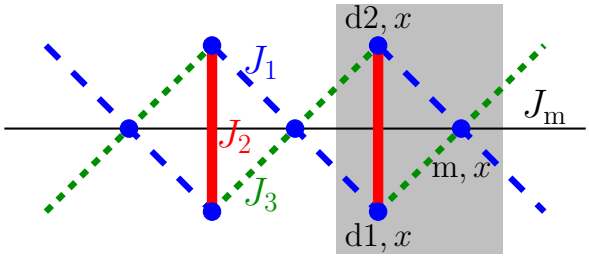

Figure 1. Generalised diamond chain model. A unit cell x (indicated by the grey shaded region) contains two dimer sites 'd1, x', 'd2, x' and one monomer site 'm, x'. These sites are connected by the exchange constants J_1, J_2, J_3 and J_m which are indicated by different line styles.

1. Introduction

On the one hand, highly frustrated magnets constitute a fascinating field of research since the competition of different interactions give rise to many exotic phenomena (see for example [1]). On the other hand, theoretical studies of highly frustrated quantum magnets are usually a notoriously difficult task, for example because the so-called 'sign problem' precludes efficient Quantum Monte Carlo simulations of such models [2]. A notable exception to this general rule are models which allow for the construction of exact ground states because of destructive quantum interference caused exactly by the frustrating interactions. A famous example is the exact dimer ground state of the two-dimensional Shastry-Sutherland model for $SrCu_2(BO_3)_2$ (see [3] for a review).

Another case of such exact eigenstates are the ground states which can be constructed exactly in terms of localised magnons in the high-field regime of certain highly frustrated quantum magnets [4–22]. Remarkably, these localised ground states give rise to a macroscopic degeneracy, i.e. a finite zero-temperature entropy exactly at the saturation field [6–9,12,13,15,16,18,19,21]. This implies an enhanced magnetocaloric effect and promises applications for efficient low-temperature cooling [7, 15, 17, 23–26].

Models with local conservation laws [9, 15, 19, 27–45] can be considered as a special mechanism to ensure the presence of localised magnons. One particular model in this category is the *ideal diamond chain* whose ground-state phase diagram was studied in [46]. This model is sketched in figure 1; the ideal diamond chain is obtained by setting $J_1 = J_3$ and $J_\mathrm{m} = 0$. In the case $J_1 = J_3$, the total spin $\vec{S}_{\mathrm{d1},x} + \vec{S}_{\mathrm{d2},x}$ of a vertical dimer is a conserved quantity in each unit cell x. Several modifications of the ideal diamond chain have also been considered in the recent literature, see, e.g. [47–52]. In particular, the '*distorted*' variant of the spin-1/2 diamond chain with $J_1 \neq J_3$ and $J_\mathrm{m} = 0$ has attracted much attention from the theoretical side [53–58]. Among the theoretical results we would like to mention in particular that a plateau at one third of the saturation magnetisation is abundant in the spin-1/2 distorted diamond chain, as can be expected for a model with a unit cell of three sites [59–61]. Evidently, it is very desirable to have an experimental realisation of a spin-1/2 distorted diamond chain,

preferably in the highly frustrated regime $J_1 \approx J_3$.

The natural mineral azurite $Cu_3(CO_3)_2(OH)_2$ was originally suggested to realise a spin-1/2 distorted diamond chain with all exchange constants antiferromagnetic [62–64], i.e. J_1, J_2, $J_3 > 0$ and $J_\mathrm{m} = 0$ in figure 1. This picture had, however, been questioned: Some authors have suggested a ferromagnetic $J_3 < 0$ [65–67] which would render the model non-frustrated whereas other authors have argued interchain coupling to be important [68]. Recent first-principles density-functional computations [69] indeed yield a three-dimensional coupling geometry with a dominant antiferromagnetic dimer exchange constant $J_2 > 0$. Nevertheless, closer inspection of the exchange geometry allows one to map this three-dimensional network effectively to the *generalised diamond chain* sketched in figure 1 [69]. A small refinement of the exchange constants obtained from the first-principles density-functional computations led to [69]

$$J_1 = 15.51\mathrm{K}\,, \qquad J_2 = 33\mathrm{K}\,, \qquad J_3 = 6.93\mathrm{K}\,, \qquad J_\mathrm{m} = 4.62\mathrm{K}\,. \tag{1}$$

Using different variants of the density-matrix renormalisation group (DMRG) method [70, 71], it was demonstrated [69] that the generalised diamond chain with the values (1) of the exchange constants is consistent with a broad range of experiments, namely the magnetisation curve [62, 72], the magnetic susceptibility [62, 69], the specific heat [62, 67, 69], the structure of the the one-third plateau as determined by NMR [73] and last but not least inelastic neutron scattering on this one-third plateau [67].

It should be noted that the parameter set (1) is not very far from the original proposal [62]. In particular, the fact that the two exchange constants J_1 and J_3 are of a comparable magnitude places azurite in a highly frustrated parameter regime. The main difference between the original parameter set [62] and (1) is the direct exchange coupling J_m between monomer spins whose presence was already suggested in [67].

In order to be precise, we present the Hamiltonian for the generalised diamond chain sketched in figure 1:

$$\begin{aligned}\mathcal{H} = \sum_{x=1}^{N/3} \Big\{ & J_1\, \vec{S}_{\mathrm{m},x} \cdot \Big(\vec{S}_{\mathrm{d2},x} + \vec{S}_{\mathrm{d1},x+1} \Big) + J_2\, \vec{S}_{\mathrm{d1},x} \cdot \vec{S}_{\mathrm{d2},x} \\ & + J_3\, \vec{S}_{\mathrm{m},x} \cdot \Big(\vec{S}_{\mathrm{d1},x} + \vec{S}_{\mathrm{d2},x+1} \Big) + J_\mathrm{m}\, \vec{S}_{\mathrm{m},x} \cdot \vec{S}_{\mathrm{m},x+1} \Big\} \\ & - g\, \mu_B\, H \sum_{x=1}^{N/3} \left(S^\mathrm{z}_{\mathrm{d1},x} + S^\mathrm{z}_{\mathrm{d2},x} + S^\mathrm{z}_{\mathrm{m},x} \right) . \end{aligned} \tag{2}$$

The total number of spins is denoted by N and x runs over the $N/3$ unit cells. The $\vec{S}_{\cdot,x}$ are spin-1/2 operators, H the external magnetic field and μ_B the Bohr magneton. In order to express the magnetic field in experimental units, we need the value of the gyromagnetic ratio g. Here we follow [69] and use $g = 2.06$ which is consistent with high-field ESR on azurite [74].

This paper is organised as follows. In section 2 we discuss two effective Hamiltonians which are obtained [56] by applying strong-coupling perturbation theory to the model (2). The two effective Hamiltonians describe the low-energy (low-temperature)

behaviour in the regime of magnetisation up to one-third and between one-third and full magnetisation, respectively. In section 3 we then compute the zero-field excitation spectrum by exact diagonalisation and a dynamical variant of the DMRG method [75]. We observe good agreement with the inelastic neutron scattering results [67], thus lending further support to the description of azurite in terms of the generalised diamond chain model (2) with the parameters (1). Next, we explore magnetocaloric properties of the model in section 4 using computations based on a transfer-matrix variant of the DMRG method [76, 77]. The zero-temperature entropy which is present in the ideal diamond chain exactly at the saturation field [15, 19] is lifted by the distortion $J_1 \neq J_3$. Nevertheless, we predict that cooling down to temperatures substantially below 1K should be possible in the high-field regime. Finally, in section 5 we summarise our findings and suggest topics for further theoretical and experimental studies of azurite.

2. Low-energy effective Hamiltonians

A simple picture of azurite is given by an effective spin-1/2 Heisenberg chain accounting for the low-energy excitations at small magnetic fields and weakly coupled dimers which describe higher energies or higher magnetic fields [62, 64, 67–69]. The corresponding effective Hamiltonians can easily be obtained from the results of [56, 69]. We will nevertheless discuss them here since they will be useful for the later analysis.

2.1. Small magnetic fields

At small magnetic fields and for large J_2 the dimers are frozen in their singlet ground state. Accordingly, the low-energy degrees of freedom are given by the monomer spins in this low-field regime. For the generalised diamond chain model, the monomer spin degrees give rise to an effective spin-1/2 chain. This description holds up to the one-third plateau where all spins of the effective spin-1/2 chain are aligned along the field direction. Because of the SU(2) symmetry present at $H = 0$, this effective spin-1/2 chain can contain only SU(2)-symmetric terms. Considering the limit $J_2 \gg |J_i|$ $(i = 1, 3)$ [56] and $H = 0$ one arrives at a nearest-neighbour Heisenberg chain

$$\mathcal{H}^{\mathrm{m}}_{\mathrm{eff.}} = J_{\mathrm{eff.}} \sum_x \vec{S}_{\mathrm{m},x} \cdot \vec{S}_{\mathrm{m},x+1} \,. \tag{3}$$

The effective exchange constant $J_{\mathrm{eff.}}$ is given up to second order in $|J_i| \ll J_2$ $(i = 1, 3)$ by [56]

$$J_{\mathrm{eff.}} = J_{\mathrm{m}} + \frac{(J_1 - J_3)^2}{2\, J_2} + \mathcal{O}\left(\left\{ \frac{J_i^3}{J_2^2} \right\} \right) . \tag{4}$$

Insertion of the values (1) for the exchange constants yields $J_{\mathrm{eff.}} \approx 5.8\mathrm{K}$.

A more accurate estimate for $J_{\mathrm{eff.}}$ can be obtained from an analysis of the spectrum on the one-third plateau where one finds two sharp excitation branches: the lower one can be attributed to the effective spin-1/2 chain and the upper one to the dimers. The numerical results [69] for these two branches at $N = 30$ are reproduced in figure 2.

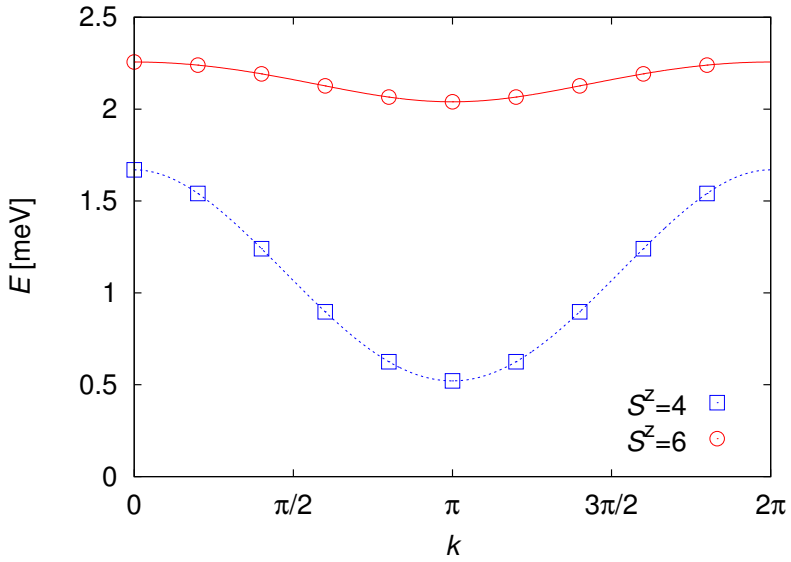

Figure 2. Excitations of the generalised diamond chain with $N = 30$ sites on the one-third plateau obtained by exact diagonalisation with $J_1 = 15.51$K, $J_2 = 33$K, $J_3 = 6.93$K, $J_{\rm m} = 4.62$K and $H = 14$T. Squares show results for $S^{\rm z} = 4$ which is just below the plateau and circles show results for $S^{\rm z} = 6$ which is just above the plateau value $S^{\rm z} = N/6 = 5$. Lines show interpolations which have been obtained by a Fourier analysis.

Lines in this figures have been obtained from a Fourier analysis of the finite-size data. From the first Fourier component of the lower branch one finds the effective exchange constant

$$J_{\rm eff.} = 6.595\text{K} \tag{5}$$

for the parameter set (1). Higher harmonics contribute less than 4% of the first harmonic to the dispersion of this lower branch, consistent with only nearest-neighbour interactions appearing in the effective Hamiltonian (3).

A consistency check on this picture is obtained by the lower edge of the one-third plateau which is located at $H_{c1} = 13.32$K according to numerical data for the generalised diamond chain model with the parameters (1) [69]. The transition at H_{c1} corresponds to the transition to saturation of the effective spin chain (3). This predicts the equality $H_{c1} = 2\, J_{\rm eff.}$ which indeed holds to high accuracy with (5).

2.2. High magnetic fields

A similar effective description holds at high magnetic fields. If J_2 is dominant and $H \approx J_2$, the monomer spins are fully polarised whereas the singlet state $|{\rm s}\rangle = \frac{1}{\sqrt{2}}\,(|\uparrow\downarrow\rangle - |\downarrow\uparrow\rangle)$ and the spin-polarised component of the triplet $|{\rm t}\rangle = |\uparrow\uparrow\rangle$ are (almost) degenerate. The collective behaviour of these dimer degrees of freedom can be efficiently

encoded by pseudo-spin-1/2 operators acting at site x

$$\begin{aligned} T^{\rm z}_x\,|{\rm s}\rangle_x &= -\frac{1}{2}\,|{\rm s}\rangle_x\,, \qquad T^{\rm z}_x\,|{\rm t}\rangle_x = \frac{1}{2}\,|{\rm t}\rangle_x\,, \\ T^{+}_x\,|{\rm s}\rangle_x &= |{\rm t}\rangle_x\,, \qquad T^{+}_x\,|{\rm t}\rangle_x = 0\,, \\ T^{-}_x\,|{\rm t}\rangle_x &= |{\rm s}\rangle_x\,, \qquad T^{-}_x\,|{\rm s}\rangle_x = 0\,. \end{aligned} \tag{6}$$

The dimer degrees of freedom give rise to another effective spin chain. However, this effective spin chain is anisotropic since the presence of an external magnetic field reduces the symmetry to U(1). In addition, corrections to the magnetic field H also need to be taken into account. Hence, the effective Hamiltonian for the $N/3$ dimer degrees of freedom is

$$\begin{aligned} \mathcal{H}^{\rm d}_{\rm eff.} = \sum_{x=1}^{N/3} \Big\{ J_{\rm z}\, T^{\rm z}_x\, T^{\rm z}_{x+1} + \frac{J_{\rm xy}}{2}\left(T^{+}_x\, T^{-}_{x+1} + T^{-}_x\, T^{+}_{x+1}\right) \Big\} \\ - (H - J_{\rm dimer}) \sum_x T^{\rm z}_x\,. \end{aligned} \tag{7}$$

The effective exchange constants can again be determined by second-order perturbation theory in $|J_i| \ll J_2$ $(i = 1, 3)$ [56]:

$$\begin{aligned} J_{\rm xy} &= \frac{(J_1 - J_3)^2}{4\,J_2} + \mathcal{O}\left(\left\{\frac{J_i^3}{J_2^2}\right\}\right)\,, \\ J_{\rm z} &= \mathcal{O}\left(\left\{\frac{J_i^3}{J_2^2}\right\}\right)\,, \\ J_{\rm dimer} &= J_2 + \frac{J_1 + J_3}{2} + \frac{(J_1 - J_3)^2}{4\,J_2} + \mathcal{O}\left(\left\{\frac{J_i^3}{J_2^2}\right\}\right)\,. \end{aligned} \tag{8}$$

In passing we note that from (4) and (8) one finds $J_{\rm xy}/J_{\rm eff.} = 1/2$ for $J_{\rm m} = 0$ and up to second order in J_1 and J_3. This ratio translates directly into the ratios of the bandwidths of the two excitation branches on the one-third plateau. However, in azurite this bandwidth ratio is measured to be about 1/6 [67]. This indicates that the excitation spectrum of azurite on the one-third plateau [67] cannot be fitted by a simple distorted diamond chain with $J_{\rm m} = 0$ [69], at least not in the region of large J_2.

Insertion of (1) into (8) yields $J_{\rm xy} = 0.56$K, $J_{\rm z} = 0$ and $J_{\rm dimer} = 44.8$K. More precise values for the effective parameters can again be derived by an analysis of numerical data [69] for the parameters (1). The first Fourier coefficient of the upper branch in figure 2 yields

$$J_{\rm xy} = 1.249{\rm K}\,. \tag{9}$$

Higher Fourier components contribute less than 7% of the first component, in agreement with only nearest-neighbour interactions appearing in (7).

The other parameters can for instance be determined from the upper edge H_{c2} of the one-third plateau and the transition to saturation at $H_{\rm sat.}$. Using $H_{c2} = J_{\rm dimer} - J_{\rm xy} - J_{\rm z}$, $H_{\rm sat.} = J_{\rm dimer} + J_{\rm xy} + J_{\rm z}$, as appropriate for (7), the numerical values [69] $H_{c2} = 43.045$K, $H_{\rm sat.} = 46.674$K and (9) we find

$$J_{\rm z} = 0.565{\rm K}\,, \qquad J_{\rm dimer} = 44.860{\rm K}\,. \tag{10}$$

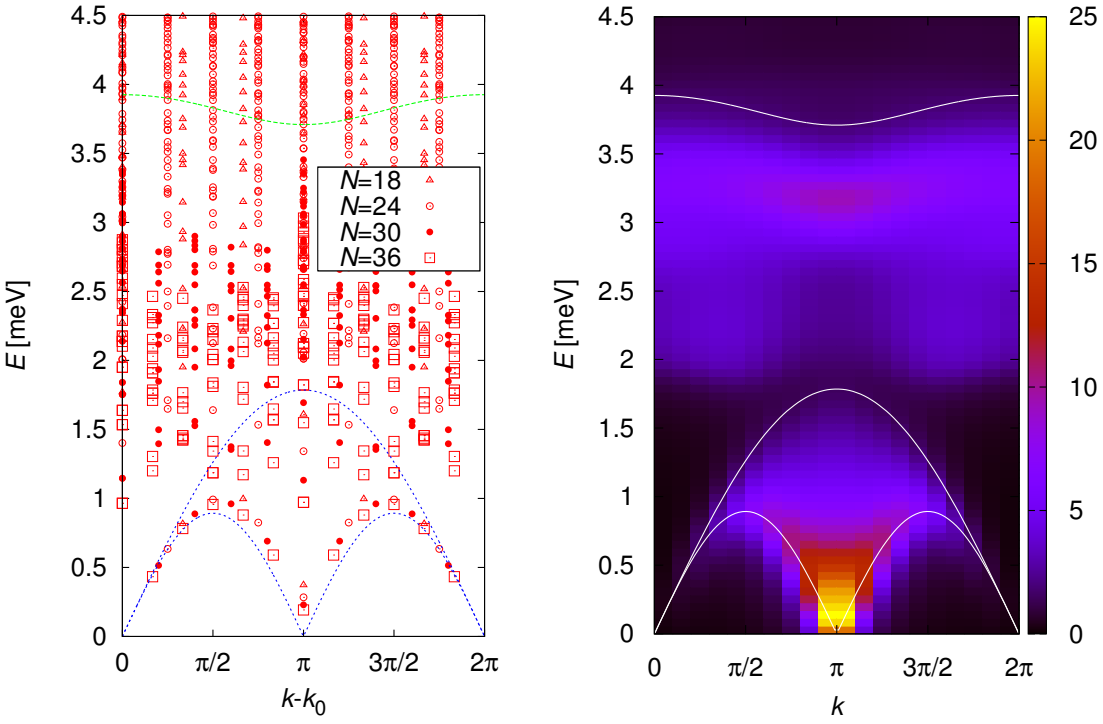

Figure 3. Zero-field spectrum of the generalised diamond chain model for azurite with the exchange constants (1). The left panel shows excitation energies E in the spin-1 sector obtained by exact diagonalisation for rings with $N = 18$, 24, 30 and 36 spins as a function of momentum $k - k_0$ where k_0 is the momentum of the ground state. The right panel shows dynamical DMRG results for the dynamic structure factor of a system with open boundary conditions and $N = 60$ sites as a function of energy E and momentum transfer k. In the latter panel, the shading corresponds to the neutron scattering intensity in arbitrary units.
In both panels lines at low energies denote the boundaries of the two-spinon continuum of an effective spin-1/2 Heisenberg chain with an effective exchange constant $J_{\text{eff.}} \approx 6.6\text{K} \approx 0.57\text{meV}$. The lines at an energy slightly below 4meV show the dimer excitation (upper branch) of figure 2 shifted up in energy by $H = 14\text{T} \approx 1.67\text{meV}$.

Two remarks are in order at this point. Firstly, we note that J_{dimer} differs substantially from the bare dimer coupling constant J_2 which can be traced to substantial first-order corrections in (8). This precludes a direct derivation of J_2 from most experimental data on azurite if accurate results are desired. Secondly, we observe that the numerical value $J_z/J_{xy} \approx 0.45$ lies in the easy-plane regime of the effective Hamiltonian (7).

A consistency check of the above analysis can be obtained from the average position of the upper branch in figure 2 which yields $J_{\text{dimer}} - J_z = 44.371\text{K}$. This agrees with (10) to better than 0.1K.

3. Excitation spectrum in zero field

The excitation spectrum on the one-third plateau found by inelastic neutron scattering on azurite [67] has been compared in [69] to computations for the generalised diamond chain model with the parameters (1) and very good agreement was found. Here we will perform a similar comparison with the experimental excitation spectrum in zero field [67].

First, we look at the spectrum itself which we have computed by exact diagonalisation for periodic chains. In this case momentum k is a good quantum number. In addition, we use conservation of total $S^{\rm z}$ as well as spin-inversion for $S^{\rm z}=0$. By virtue of the Wigner-Eckart theorem, inelastic neutron scattering on the ground state of an SU(2)-symmetric antiferromagnet is sensitive only to excitations with total spin 1 [78]. Therefore we reconstruct the total spin quantum numbers from the $S^{\rm z}$- and spin-inversion-resolved results. For $N=18$ spins it is possible to perform a full diagonalisation. For $N=24$ sites we have used the method described in section 2.1 of [79] to compute a large number of low-lying energies. Finally, for $N=30$ and 36 we have used Spinpack (see `http://www-e.uni-magdeburg.de/jschulen/spin/index.html`). The left panel of figure 3 shows the results of these computations for the spin-1 sector. For $N=18$ and 24 we have sufficiently many states to cover the shown energy range completely. However, for $N=30$ and 36 it is impossible to compute so many states accurately. Therefore, for $N=30$ and 36 we had to restrict to lower energies $E\lesssim 2.8$meV and 2.4meV, respectively. Accordingly, one should keep in mind that eigenvalues are missing in the left panel of figure 3 at higher energies for the two biggest system sizes.

One can discern some structure in the spectrum of the left panel of figure 3 at low energies which we will discuss below. However, at energies $E\gtrsim 1.5$meV, there is a large density of spin-one excitations without any evident structure. In order to understand which excitations can be observed by neutrons, we therefore need to compute the dynamic structure factor

$$S^{\rm xx}(\vec{k},\omega)=\frac{3}{N}\sum_{\langle x,y\rangle}{\rm e}^{i\,\vec{k}\cdot(\vec{R}_x-\vec{R}_y)}\;{\rm Im}\langle 0|S^{\rm x}_x\frac{1}{\omega+E_0-\mathcal{H}+i\,\eta}S^{\rm x}_y|0\rangle\,. \tag{11}$$

We have computed this dynamic structure factor via the correction-vector method in the density-matrix renormalisation group (DMRG) following [75]. First, we have calculated the spectral function between each pair of sites in the chain

$$G_{x,y}(\omega)=\langle 0|S^{\rm x}_x\frac{1}{\omega+E_0-\mathcal{H}+i\,\eta}S^{\rm x}_y|0\rangle \tag{12}$$

using 2 sweeps for each frequency point ω, $N=60$ lattice sites and $m=200$ kept states. For technical reason one has to introduce a Lorentzian broadening $\eta>0$ of the spectral function. We choose $\eta=0.05\,J_2$.

In a second step, one needs to Fourier transform $G_{x,y}$ in order to obtain the dynamic structure factor (11). The diamond chain contains dimers which are coupled strongly by J_2. The structure factor of a dimer is known to depend strongly on the momentum

transfer and to lead to vanishing intensity at zero momentum transfer along the dimer direction [80]. It is therefore important to use the precise positions $\vec{R}_x$ of the spin-1/2 copper atoms in azurite [81] as well as the experimental value of the momentum transfer transverse to the chains [67] when evaluating (11) from $G_{x,y}$. The result of this procedure is shown in the right panel of figure 3. The main limiting factor of the resolution in this panel is a finite resolution of the momentum transfer k along the chain direction which is caused by the open ends of the chain.

The calculated structure factor shown in the right panel of figure 3 shares the following features with the results obtained by inelastic neutron scattering on azurite [67]: (i) There is a scattering continuum at energies $E \lesssim 2$meV with a sharp lower edge. (ii) At higher energies, one finds a broad band of excitations with a sharp feature in its middle. Just the energy of this feature differs between the model where it is located at $E \approx 3.2$meV and the experiment [67] which finds it at $E \approx 6$meV.

For a more quantitative analysis of the low-energy features we can use the effective spin-chain Hamiltonian introduced in section 2.1. It is well known that the low-energy excitations of a spin-1/2 Heisenberg chain form a two-spinon continuum whose boundaries are given by [78, 82, 83]

$$\epsilon_{\mathrm{l}} = \frac{\pi}{2}\, J_{\mathrm{eff.}}\, |\sin k| \;, \qquad \epsilon_{\mathrm{u}} = \pi\, J_{\mathrm{eff.}}\, \sin\frac{k}{2}\,. \tag{13}$$

The boundaries of the two-spinon continuum with the value of $J_{\mathrm{eff.}}$ given by (5) are shown by the lines in figure 3 and one observes that the low-energy excitations fall indeed into this region. One can also directly compare the lowest excitations in the left panel of figure 3 with those of a spin-1/2 chain with $N/3$ sites [78, 82] and one observes again good agreement. Furthermore, even the low-energy part of the dynamic structure factor shown in the right panel of figure 3 matches nicely with that of a spin-1/2 Heisenberg chain [84, 85]. Hence we conclude that an effective spin-1/2 Heisenberg chain with $J_{\mathrm{eff.}}$ given by (5) describes the low-energy properties of the generalised diamond chain well.

The location of the dimer branch can be estimated by adding the Zeeman energy $H = 14\mathrm{T} \approx 1.67$meV to the upper branch in figure 2. This yields the curves in figure 3 slightly below 4meV. The shape of this curve traces the dispersion of the broad maximum between 3 and 3.5meV in the right panel of figure 3 nicely, but it is about 0.5meV too high in energy. Indeed, by applying a simple Zeeman shift to the upper branch of figure 2, we are stretching the high-field effective Hamiltonian (7) well beyond its limits of validity. After all, there are many low-energy excitations at $H = 0$ which are not taken into account by this Hamiltonian. Renormalisation of the bare dimer excitation by many-body effects is therefore expected. This is reflected both by the broad diffusive background and a down-shift of the maximum scattering intensity by about 0.5meV in the generalised diamond chain model with respect to the effective Hamiltonian (7) (see right panel of figure 3). It should be noted that the experiments [67] on azurite observe a renormalisation of the bare dimer excitation to higher energies rather than lower energies as in our model. This is likely to be a signature of the three-dimensional ordered state in which the experiments were performed. Accordingly we speculate that

quantitative agreement could be improved by taking the three-dimensional coupling geometry [69] fully into account.

In any case, analysis of the low-energy excitation spectrum of azurite [67] supports the conclusion [69] that the generalised diamond chain model with the parameters (1) yields a good overall description of the experimental situation.

4. Magnetocaloric effect in high magnetic fields

One of the interesting features of azurite is its proximity to a class of systems with localised magnons at high magnetic fields giving rise to an enhanced magnetocaloric effect [19].

4.1. Ideal diamond chain

Let us first take a look at an ideal diamond chain model with parameters which are similar to those for azurite. Note that for $J_1 = J_3$ one can use conservation of the total spin on each vertical dimer $\vec{S}_{\mathrm{d1},x} + \vec{S}_{\mathrm{d2},x}$ to speed up the computation [19]. Figure 4 shows the result for $N = 24$ spins and $J_1 = J_3$, $J_2 = 3\,J_1$. The large value of J_2 ensures that all low-energy states are simple product states. Hence, finite-size effects are negligible in figure 4.

In a magnetic field the monomer spins are immediately polarised and thus frozen. Exactly at the saturation field $H_{\mathrm{sat.}}$, the dimer singlet and one component of the dimer triplet become degenerate, giving rise to a two-fold degeneracy per dimer, i.e. a residual entropy $S/N = (\ln 2)/3$ [15, 19]. On the other hand, for low magnetic fields the dimers are frozen in their singlet state. Exactly at $H = 0$, the two projections of the monomer spins become degenerate and we find again a residual entropy $S/N = (\ln 2)/3$. This particular value of the entropy is traced by the white lines in figure 4. Consider now an adiabatic process which is defined by a constant entropy and thus follows the lines in figure 4. If such an adiabatic process is started below the white lines in figure 4, i.e. with an entropy $S/N < (\ln 2)/3$, one achieves cooling to $T \to 0$ for $H \to H_{\mathrm{sat.}}$ (or for $H \to 0$).

4.2. Generalised diamond chain model for azurite

Now we turn to the generalised diamond chain model for azurite and check how $J_1 \neq J_3$ lifts the degeneracy. For this purpose we have computed the entropy using a transfer-matrix variant of the density-matrix renormalisation group, also known as 'TMRG' [76, 77]. Note that this method works for the infinite system and proceeds at a fixed magnetic field H from high to low temperatures by successively adding Trotter-Suzuki slices. There is just one refinement which had to be implemented to get accurate results at low temperatures and high magnetic fields. In this region, the (asymmetric) reduced density matrix only has a small number of large eigenvalues while all other eigenvalues are tiny. Therefore, we use an additional reorthogonalisation procedure

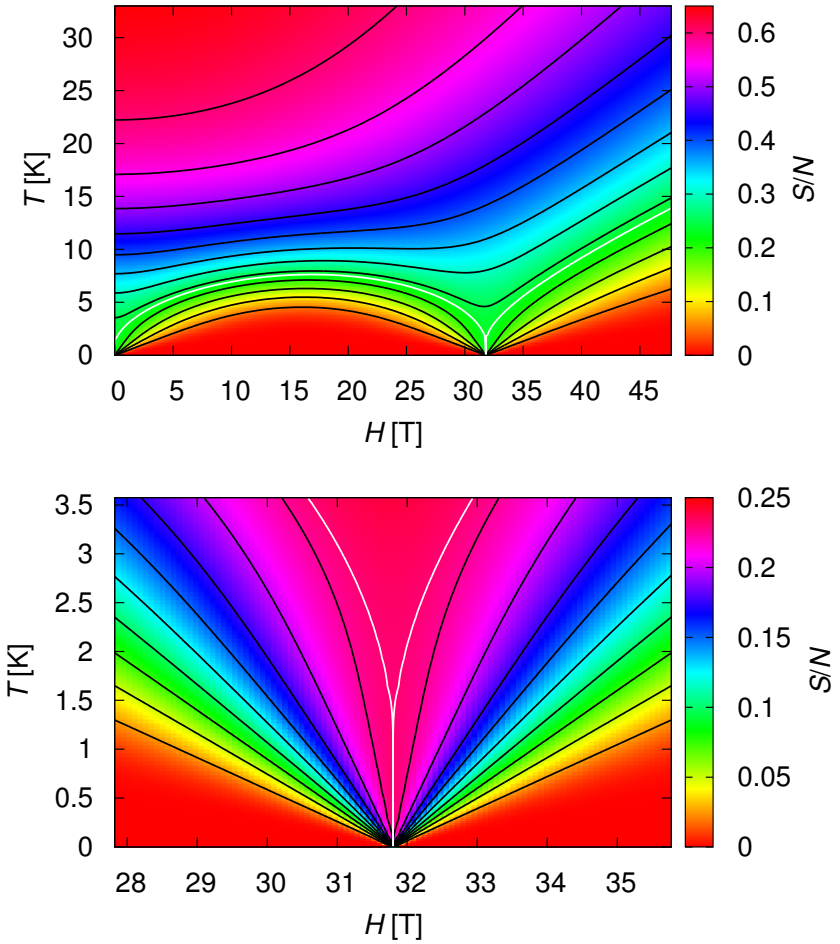

Figure 4. Entropy per spin S/N of the ideal diamond chain model with $J_1 = J_3 = 11\text{K}$, $J_2 = 33\text{K}$ and $J_\text{m} = 0$, as a function of magnetic field H and temperature T. The top panel covers the region from zero field to a fully polarised system. In this panel the black lines correspond to $S/N = 0.05, 0.1, 0.15, \ldots$ (in increasing order). The bottom panel focuses on the low-temperature behaviour at the transition to full polarisation. Here the black lines correspond to $S/N = 0.025, 0.05, 0.075, \ldots$ The white lines in both panels denote the residual entropy $S/N = (\ln 2)/3$.
The data in this figure has been obtained by exact diagonalisation for $N = 24$ spins.

after the left and right eigenvectors of the reduced density matrix are obtained by exact diagonalisation. This allows us to keep more states and thus improve accuracy. We have tested this procedure against exact results for the entropy of the spin-1/2 Heisenberg chain [86] and found excellent agreement.

Figure 5 shows the result for the entropy of the generalised diamond chain with the parameters (1). In this case none of the constant entropy curves with $S/N > 0$ goes to $T = 0$, reflecting the lifting of the degeneracy present in the ideal diamond chain. In other words: in the present case the entropy per site S/N goes to zero as $T \to 0$ for *all values of the magnetic field* H. The value of the residual entropy of the ideal diamond

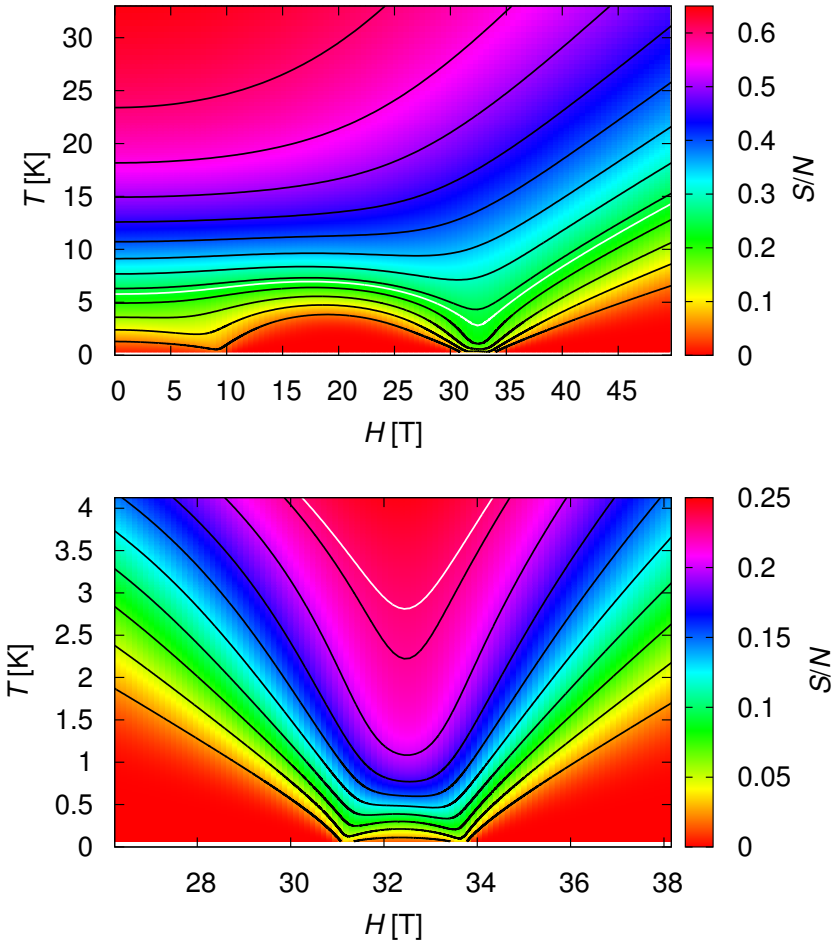

Figure 5. Entropy per spin S/N of the generalised diamond chain model for azurite, i.e. $J_1 = 15.51$K, $J_2 = 33$K, $J_3 = 6.93$K and $J_\mathrm{m} = 4.62$K, as a function of magnetic field H and temperature T. The top panel covers the region from zero field to a fully polarised system. In this panel the black lines correspond to $S/N = 0.05$, 0.1, 0.15, ... (in increasing order). The bottom panel focuses on the low-temperature behaviour at the transition to full polarisation. Here the black lines correspond to $S/N = 0.025$, 0.05, 0.075, ... The white lines in both panels denote the residual entropy of the ideal diamond chain, $S/N = (\ln 2)/3$.
The data in this figure is for the thermodynamic limit and has been obtained by TMRG with $m = 300$ kept states.

chain $S/N = (\ln 2)/3$ is again shown by white lines in figure 5. One can read off that this residual entropy is pushed up to $T > 2.8$K.

The degeneracy at $H = 0$ is particularly fragile. It is lifted not only by a distortion $J_1 \neq J_3$, but also by a finite direct coupling of the monomer spins $J_\mathrm{m} > 0$. This is reflected by a window of $H_{c1} \approx 9.6$T for the polarisation of the monomer spins [69] and the fact that the value $S/N = (\ln 2)/3$ is pushed up to $T \approx 5.8$K for $H = 0$ (compare the upper panel of figure 5).

On the other hand, the degeneracy at the saturation field would survive a finite

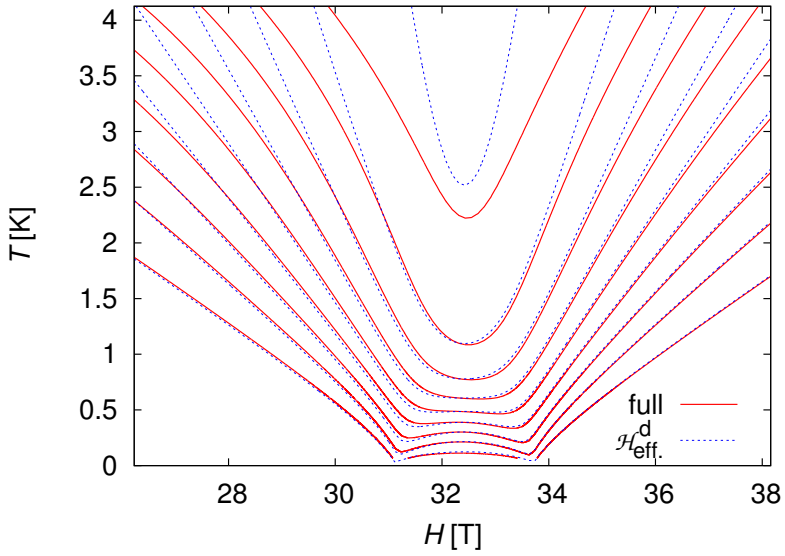

Figure 6. Constant-entropy curves of the full generalised diamond chain model (full lines) in comparison to those of the effective Hamiltonian (7) (dashed lines). Lines correspond to $S/N = 0.025,\ 0.05,\ 0.075,\ \ldots$ (in increasing order). Results for the generalised diamond chain model correspond to the black constant entropy curves in the lower panel of figure 5. The entropy of the effective Hamiltonian (7) has been computed by exact diagonalisation with the parameters (9), (10) and $N/3 = 20$ dimer sites. This system size is large enough to ensure the absence of visible finite-size effects in the figure.

monomer-monomer coupling $J_{\rm m} > 0$ and is lifted only by the distortion $J_1 \neq J_3$. Accordingly the region in which the dimers are polarised is spread over a smaller field window of about $\Delta H = 2.6$T width between $H_{c2} = 31.1$T and $H_{\rm sat.} = 33.7$T [69] and the value $S/N = (\ln 2)/3$ is attained already for $T \approx 2.8$K (see the lower panel of figure 5). Although the entropy $S/N = (\ln 2)/3$ is spread over a temperature window of approximately 2.8K, an adiabatic process can still cool to substantially lower temperatures in this high-field region. For example, an adiabatic process which starts at $(H, T) \approx (27\text{T}, 1.6\text{K})$ or $(38\text{T}, 1.65\text{K})$ would go down to $T < 70$mK as $H \to 31.1$T or 33.8T, respectively. This case corresponds to an entropy $S/N = 0.025$, i.e. the lowest curve in the bottom panel of 5. For the larger value $S/N = 0.05$ (second curve in the lower panel of figure 5) an adiabatic process would still cool to a minimum temperature $T \approx 90$mK.

Finally, we compare the entropy in the high-field region shown in the lower panel of figure 5 with the entropy of the effective Hamiltonian (7). The latter can be considered as an effective description of the splitting of the manifold of the $2^{N/3}$ states which are degenerate in the ideal diamond chain exactly at $H_{\rm sat.}$.

In principle, the entropy could be computed exactly for the model (7) [86]. However, we found it simpler to perform a full diagonalisation of this model with the parameters (9), (10) and $N/3 = 20$ dimer sites. This system size is large enough to ensure the

absence of visible finite-size effects in the dashed constant-entropy curves in figure 6.

The constant entropy curves of the full model which are shown by black lines in the lower panel of figure 5 are reproduced in figure 6 by full lines. The dashed lines show results for the effective Hamiltonian (7) with the same values of the entropy S/N. One finds that the effective model reproduces the results of the full one well for temperatures $T \lesssim 1.5$K and in the high-field regime shown in figure 6. The deviations observed at higher temperatures in figure 6 indicate that other states become relevant in this temperature range. Note that the uppermost curve in figure 6 corresponds to $S/N = 0.225$ which is very close to the total entropy $S/N = (\ln 2)/3$ of the effective chain model. Still, a simplified description in terms of the effective Hamiltonian (7) works well in high magnetic fields and at sufficiently low temperatures.

5. Summary and discussion

In this work we have explored further properties of the generalised diamond chain model for azurite [69]. First, we have computed the excitation spectrum in the absence of a magnetic field and found a two-spinon continuum at low energies as well as a dimer branch sitting on a broad background at higher energies. These features are in good agreement with inelastic neutron scattering results on azurite [67], thus further supporting the description of azurite in terms of a generalised diamond chain model [69].

We have then computed magnetocaloric properties at high magnetic fields. The degeneracy present in the ideal model at the saturation field [15, 19] is lifted in the generalised diamond chain model for azurite. Still, we predict cooling capabilities down to temperatures substantially below 1K as the magnetic field approaches the upper edge of the one-third plateau H_{c2} or the saturation field $H_{\text{sat.}}$ from below or above, respectively.

There are at least two features in azurite which are not accounted for by the generalised diamond chain model. Firstly, a magnetic anisotropy is clearly present in azurite [62]. This is most likely due to Dzyaloshinsky-Moriya interactions. Indeed, there is at least one investigation of the effect of such terms [87], however not for the parameters which we consider to be most appropriate for azurite. On the other hand, the complication of magnetic anisotropies can be experimentally avoided by aligning the external magnetic field with the high-symmetry axis.

Secondly, azurite orders for temperatures below 2K in low magnetic fields [62, 88–91]. This ordering process reflects the presence of interchain coupling terms [68, 69] and could account in particular for the fact that we predict the dimer branch at zero magnetic field at energies which are a few meV below the experimental result [67]‡. Also in high magnetic fields azurite is found to be ordered at $T = 600$mK [93]. Such an ordering transition will push most of the low-temperature entropy up to the transition temperature such that most of the adiabatic (de)magnetisation curves are pushed to

‡ Interchain coupling and magnetic anisotropies can also give rise to additional finer structures in the spectra which are visible in high-resolution inelastic neutron scattering experiments [92].

temperatures higher than 600mK. Nevertheless, the ordering temperature is expected to vanish as one approaches the one-third plateau and the fully polarised state at $H = H_{c2}$ and $H_{\mathrm{sat.}}$, respectively. Thus, we expect the strong cooling effect at H_{c2} and $H_{\mathrm{sat.}}$ to be preserved in azurite as these two fields are approached from below and above, respectively.

A more accurate treatment of the interchain coupling geometry [69] is clearly necessary for a quantitative description of the ordered states of azurite at temperatures below 2K. In this context, it may be interesting to note that we can obtain very accurate results using effective Hamiltonians, provided that their parameters are determined carefully. On the one hand, we have shown that the effective Heisenberg chain (3) yields a very good description of the low-energy excitations at $H = 0$ (see figure 3). On the other hand, figure 6 demonstrates that the low-temperature behaviour of the generalised diamond chain in high magnetic fields is well described by the effective Hamiltonian (7). The high frustration of the underlying model is reflected by the small values of the effective exchange constants J_{xy} and J_{z} which are one to two orders of magnitude smaller than the bare exchange constants.

In particular, the experimental observation of simple antiferromagnetic order in azurite at high magnetic fields [93] can be rationalised by noting that the parameters (9) and (10) lead to an effective easy-plane anisotropy. Under such conditions an instability towards antiferromagnetic order in the transverse components is expected. However, for a quantitative description of the low-energy properties of azurite in the high-field region, interchain coupling definitely needs to be included in an effective Hamiltonian, in particular in view of the fact that the effective one-dimensional exchange constant (9) is comparable to the maximal ordering temperature in the high-field regime [93].

Similar effective Hamiltonians have been successfully employed, e.g., in the context of $SrCu_2(BO_3)_2$ [94]. However, the model for azurite [69] has the advantage that the bare dimer exchange constant J_2 is substantially bigger than any other exchange constant. Hence, we may not only expect less terms to be relevant in the effective Hamiltonians than in the case of $SrCu_2(BO_3)_2$ [94], but also better quantitative validity for the parameters appropriate to azurite [69] if the parameters of the effective models are determined carefully.

Finally, we note that the magnetocaloric effect has been widely used at a qualitative level for the experimental determination of the phase diagram of spin systems in a magnetic field (see, e.g., [95–101]) and there is indirect evidence for a strong magnetocaloric effect in $SrCu_2(BO_3)_2$ [102]. However, as far as we are aware, there are only very few quantitative measurements of the cooling capabilities of quantum spin systems [103, 104] and in particular highly frustrated magnets [24, 105]. Measurements of the magnetocaloric effect in the high-field region of azurite would therefore certainly be very interesting.

Acknowledgments

We are grateful to M. Horvatić and K. Rule for useful discussions and comments. We acknowledge allocation of the CPU time on the High Performance Computer Cluster "Kohn" in the Department of Physics, Renmin University of China as well as the Theory/Grid Cluster at Göttingen University. A.H. and J.R. would like to thank the DFG for financial support via a Heisenberg fellowship under project HO 2325/4-2 and under project RI615/16-1, respectively. S.H. would like to acknowledge support via a LiSUM fellowship as well as by grants NSFC10874244 and MSTC2007CB925001. R.P. is supported by the Japan Society for the Promotion of Science (JSPS) and the Alexander von Humboldt-Foundation.

References

[1] Lacroix C, Mendels P and Mila F 2011 Introduction to Frustrated Magnetism (*Springer Series in Solid-State Sciences* vol. 164) (Heidelberg: Springer)
[2] Troyer M and Wiese U-J 2005 *Phys. Rev. Lett.* **94** 170201
[3] Miyahara S and Ueda K 2003 *J. Phys.: Condens. Matter* **15** R327
[4] Schnack J, Schmidt H-J, Richter J and Schulenburg J 2001 *Eur. Phys. J.* B **24** 475
[5] Schulenburg J, Honecker A, Schnack J, Richter J and Schmidt H-J 2002 *Phys. Rev. Lett.* **88** 167207
[6] Richter J, Schulenburg J and Honecker A 2004 *Lect. Notes Phys.* **645** 85
[7] Zhitomirsky ME and Honecker A 2004 *J. Stat. Mech.: Theor. Exp.* P07012
[8] Zhitomirsky ME and Tsunetsugu H 2004 *Phys. Rev.* B **70** 100403(R)
[9] Derzhko O and Richter J 2004 *Phys. Rev.* B **70** 104415
[10] Richter J, Schulenburg J, Honecker A and Schmalfuß D 2004 *Phys. Rev.* B **70** 174454
[11] Richter J, Derzhko O and Schulenburg J 2004 *Phys. Rev. Lett.* **93** 107206
[12] Richter J, Schulenburg J, Honecker A, Schnack J and Schmidt H-J 2004 *J. Phys.: Condens. Matter* **16** S779
[13] Zhitomirsky ME and Tsunetsugu H 2005 *Prog. Theor. Phys. Suppl.* **160** 36
[14] Schmidt R, Richter J and Schnack J 2005 *J. Magn. Magn. Mater.* **295** 164
[15] Derzhko O and Richter J 2006 *Eur. Phys. J.* B **52** 23
[16] Schnack J, Schmidt H-J, Honecker A, Schulenburg J and Richter J 2006 *J. Phys.: Conf. Ser.* **51** 43
[17] Schnack J, Richter J and Schmidt R 2007 *Phys. Rev.* B **76** 054413
[18] Zhitomirsky ME and Tsunetsugu H 2007 *Phys. Rev.* B **75** 224416
[19] Derzhko O, Richter J, Honecker A and Schmidt H-J 2007 *Low Temp. Phys.* **33** 745
[20] Rousochatzakis I, Läuchli AM and Mila F 2008 *Phys. Rev.* B **77** 094420
[21] Richter J, Derzhko O and Honecker A 2008 *Int. Jour. Mod. Phys. B* **22** 4418
[22] Schnack J 2010 *Dalton Trans.* **39** 467
[23] Zhitomirsky ME 2003 *Phys. Rev.* B **67** 104421
[24] Sosin SS, Prozorova LA, Smirnov AI Golov AI, Berkutov IB, Petrenko OA, Balakrishnan G and Zhitomirsky ME 2005 *Phys. Rev.* B **71** 094413
[25] Honecker A and Zhitomirsky ME 2009 *J. Phys.: Conf. Ser.* **145** 012082
[26] Pereira MSS, de Moura FABF and Lyra ML 2009 *Phys. Rev.* B **79** 054427
[27] Gelfand MP 1991 *Phys. Rev.* B **43** 8644
[28] Ivanov NB and Richter J 1997 *Phys. Lett.* A **232** 308
[29] Richter J, Ivanov NB and Schulenburg J 1998 *J. Phys.: Condens. Matter* **10** 3635
[30] Mambrini M, Trébosc J and Mila F 1999 *Phys. Rev.* B **59** 13806
[31] Koga A, Okunishi K and Kawakami N 2000 *Phys. Rev.* B **62** 5558

[32] Honecker A, Mila F and Troyer M, *Eur. Phys. J.* B **15** 227
[33] Müller-Hartmann E, Singh RRP, Knetter C and Uhrig GS 2000 *Phys. Rev. Lett.* **84** 1808
[34] Gros C, Valentí R, Alvarez JV, Hamacher K and Wenzel W 2000 *Phys. Rev.* B **62** R14617
[35] Trebst S and Sengupta S 2000 *Phys. Rev.* B **62** R14613
[36] Honecker A and Brenig W 2001 *Phys. Rev.* B **63** 144416
[37] Chattopadhyay E and Bose I 2002 *Phys. Rev.* B **65** 134425
[38] Schulenburg J and Richter J 2002 *Phys. Rev. B* **65** 054420
[39] Schulenburg J and Richter J 2002 *Phys. Rev.* B **66** 134419
[40] Chen S and Büttner H 2002 *Eur. Phys. J.* B **29** 15
[41] Rojas O and Alcaraz F C 2003 *Phys. Rev.* B **67** 174401
[42] Richter J, Derzhko O and Krokhmalskii T 2006 *Phys. Rev.* B **74** 144430
[43] Bergman DL, Wu C and Balents L 2008 *Phys. Rev.* B **78** 125104
[44] Manmana SR, Picon J-P, Schmidt KP and Mila F 2010 Unconventional magnetization plateaus in a Shastry-Sutherland spin tube *Preprint* arXiv:1003.1696
[45] Derzhko O, Krokhmalskii T and Richter J 2010 *Phys. Rev.* B **82** (2010) 214412
[46] Takano K, Kubo K and Sakamoto H 1996 *J. Phys.: Condens. Matter* **8** 6405
[47] Čanova L, Strečka J and Jaščur M 2006 *J. Phys.: Condens. Matter* **18** 4967
[48] Čanova L, Strečka J and Lučivjanský T 2009 *Condensed Matter Physics* **12** 353
[49] Ivanov NB, Richter J and Schulenburg J 2009 *Phys. Rev.* B **79** 104412
[50] Hida K, Takano K and Suzuki H 2010 *J. Phys. Soc. Japan* **79** 044702
[51] Hida K, Takano K and Suzuki H 2010 *J. Phys. Soc. Japan* **79** 114703
[52] Rojas O, de Souza SM, Ohanyan V and Khurshudyan M 2011 *Phys. Rev.* B **83** 094430
[53] Okamoto K, Tonegawa T, Takahashi Y and Kaburagi M 1999 *J. Phys.: Condens. Matter* **11** 10485
[54] Tonegawa T, Okamoto K, Hikihara T, Takahashi Y and Kaburagi M 2000 *J. Phys. Soc. Japan* **69** Suppl. A 332
[55] Tonegawa T, Okamoto K, Hikihara T, Takahashi Y and Kaburagi M 2001 *J. Phys. Chem. Solids* **62** 125
[56] Honecker A and Läuchli A 2001 *Phys. Rev.* B **63** 174407
[57] Okamoto K, Tonegawa T and Kaburagi M 2003 *J. Phys.: Condens. Matter* **15** 5979
[58] Sakai T, Okamoto K and Tonegawa T 2009 *J. Phys.: Conf. Ser.* **145** 012065
[59] Oshikawa M, Yamanaka M and Affleck I 1997 *Phys. Rev. Lett.* **78** 1984
[60] Cabra DC, Honecker A and Pujol P 1997 *Phys. Rev. Lett.* **79** 5126
[61] Cabra DC, Honecker A and Pujol P 1998 *Phys. Rev.* B **58** 6241
[62] Kikuchi H, Fujii Y, Chiba M, Mitsudo S, Idehara T, Tonegawa T, Okamoto K, Sakai T, Kuwai T and Ohta H 2005 *Phys. Rev. Lett.* **94** 227201
[63] Kikuchi H, Fujii Y, Chiba M, Mitsudo S, Idehara T, Tonegawa T, Okamoto K, Sakai T, Kuwai T and Ohta H 2006 *Phys. Rev. Lett.* **97** 089702
[64] Mikeska H-J and Luckmann C 2008 *Phys. Rev.* B **77** 054405
[65] Gu B and Su G 2006 *Phys. Rev. Lett.* **97** 089701
[66] Gu B and Su G 2007 *Phys. Rev.* B **75** 174437
[67] Rule KC, Wolter AUB, Süllow S, Tennant DA, Brühl A, Köhler S, Wolf B, Lang M and Schreuer J 2008 *Phys. Rev. Lett.* **100** 117202
[68] Kang J, Lee C, Kremer RK and Whangbo M-H 2009 *J. Phys.: Condens. Matter* **21** 392201
[69] Jeschke H, Opahle I, Kandpal H, Valentí R, Das H, Saha-Dasgupta T, Janson O, Rosner H, Brühl A, Wolf B, Lang M, Richter J, Hu S, Wang X, Peters R, Pruschke T and Honecker A 2010 Multi-step approach to microscopic models for frustrated quantum magnets – the case of the mineral azurite *Preprint* arXiv:1012.1090, to appear in *Phys. Rev. Lett.*
[70] White SR 1992 *Phys. Rev. Lett.* **69** 2863
[71] Schollwöck U 2005 *Rev. Mod. Phys.* **77** 259
[72] Kikuchi H, Fujii Y, Chiba M, Mitsudo S, Idehara T, Tonegawa T, Okamoto K, Sakai T, Kuwai T, Kindo K, Matsuo A, Higemoto W, Nishiyama K, Horvatić M and Berthier C 2005 *Progr. Theor.*

Phys. Suppl. **159** 1
[73] Aimo F, Krämer S, Klanjšek M, Horvatić M, Berthier C and Kikuchi H 2009 *Phys. Rev. Lett.* **102** 127205
[74] Ohta H, Okubo, S, Kamikawa T, Kunimoto T, Inagaki Y, Kikuchi H, Saito T, Azuma M and Takano M 2003 *J. Phys. Soc. Japan* **72** 2464
[75] Jeckelmann E 2002 *Phys. Rev.* B **66** 045114
[76] Bursill R J, Xiang T and Gehring GA 1996 *J. Phys.: Condens. Matter* **8** L583
[77] Wang X and Xiang T 1997 *Phys. Rev.* B **56** 5061
[78] Müller G, Thomas H, Beck H and Bonner JC 1981 *Phys. Rev.* B **24** 1429
[79] Honecker A and Wessel S 2009 *Condensed Matter Physics* **12** 399
[80] Furrer A and Güdel H-U 1979 *J. Magn. Magn. Mater.* **14** 256
[81] Zigan F and Schuster HD 1972 *Z. Kristallogr.* **135** 416.
[82] des Cloizeaux J and Pearson JJ 1962 *Phys. Rev.* **128** 2131 (1962)
[83] Faddeev LD and Takhtajan LA 1981 *Phys. Lett.* A **85** 375
[84] Lake B, Tennant DA, Frost CD and Nagler SE 2005 *Nature Materials* **4** 329
[85] Caux J-S and Hagemans R 2006 *J. Stat. Mech.: Theor. Exp.* P12013
[86] Trippe C, Honecker A, Klümper A and Ohanyan V 2010 *Phys. Rev.* B **81** 054402
[87] Sakai T, Okamoto K and Tonegawa T 2010 *J. Phys.: Conf. Ser.* **200** 022052
[88] Spence RD and Ewing RD 1958 *Phys. Rev.* **112** 1544
[89] Forstat H, Taylor G and King RB 1959 *J. Chem. Phys.* **31** 929
[90] Gibson MCR, Rule KC, Wolter AUB, Hoffmann J-U, Prokhnenko O, Tennant DA, Gerischer S, Kraken M, Litterst FJ, Süllow S, Schreuer J, Luetkens H, Brühl A, Wolf B and Lang M 2010 *Phys. Rev.* B **81** 140406(R)
[91] Rule KC, Reehuis M, Gibson MCR, Ouladdiaf B, Gutmann MJ, Hoffmann J-U, Gerischer S, Tennant DA, Süllow S and Lang M 2011 *Phys. Rev.* B **83** 104401
[92] Rule KC 2011 *private communication*
[93] Aimo F, Krämer S, Klanjšek, Horvatić M and Berthier C 2011 Magnetic structure of azurite above the 1/3 magnetization plateau *Preprint* arXiv:1103.0376
[94] Dorier J, Schmidt KP and Mila F 2008 *Phys. Rev. Lett.* **101** 250402
[95] Jaime M, Correa VF, N. Harrison, Batista CD, Kawashima N, Kazuma Y, Jorge GA, Stern R, Heinmaa I, Zvyagin SA, Sasago Y and Uchinokura K 2004 *Phys. Rev. Lett.* **93** 087203
[96] Samulon EC, Jo Y-J, Sengupta P, Batista CD, Jaime M, Balicas L and Fisher IR 2008 *Phys. Rev.* B **77** 214441
[97] Rüegg Ch, Kiefer K, Thielemann B, McMorrow DF, Zapf V, Normand B, Zvonarev MB, Bouillot P, Kollath C, Giamarchi T, Capponi S, Poilblanc D, Biner D and Krämer KW 2008 *Phys. Rev. Lett.* **101** 247202
[98] Fortune NE, Hannahs ST, Yoshida Y, Sherline TE, Ono T, Tanaka H and Takano Y 2009 *Phys. Rev. Lett.* **102** 257201
[99] Samulon EC, Kohama Y, McDonald RD, Shapiro MC, Al-Hassanieh KA, Batista CD, Jaime M and Fisher IR 2009 *Phys. Rev. Lett.* **103** 047202
[100] Aczel AA, Kohama Y, Jaime M, Ninios K, Chan HB, Balicas L, Dabkowska HA and Luke GM 2009 *Phys. Rev.* B **79** 100409(R)
[101] Aczel AA, Kohama Y, Marcenat C, Weickert F, Jaime M, Ayala-Valenzuela OE, McDonald RD, Selesnic SD, Dabkowska HA and Luke GM 2009 *Phys. Rev. Lett.* **103** 207203
[102] Levy F, Sheikin I, Berthier C, Horvatić M, Takigawa M, Kageyama H, Waki T and Ueda Y 2008 *Europhys. Lett.* **81** 67004
[103] Lang M, Tsui Y, Wolf B, Jaiswal-Nagar D, Tutsch U, Honecker A, Remović-Langer K, Prokofiev A, Assmus W and Donath G 2010 *J. Low Temp. Phys.* **159** 88
[104] Wolf B, Tsui Y, Jaiswal-Nagar D, Tutsch U, Honecker A, Remović-Langer K, Hofmann G, Prokofiev A, Assmus W, Donath G and Lang M 2011 Magnetocaloric effect and magnetic cooling near a field-induced quantum-critical point *PNAS* DOI: 10.1073/pnas.1017047108 (*Preprint*

arXiv:1012.3328)
[105] Radu T, Tokiwa Y, Coldea R, Gegenwart P, Tylczynski Z and Steglich F 2007 *Sci. Technol. Adv. Mater.* **8** 406